Effect of C additions to the microstructure and wear behaviour of CoCrFeNi highentropy alloy

Zeling Zhang, Yanfang Ling, Jia Hui, Fei Yang, Xuhai Zhang, Shuyong Tan, Zonghan Xie, Feng Fang

PII: S0043-1648(23)00415-5

DOI: https://doi.org/10.1016/j.wear.2023.205032

Reference: WEA 205032

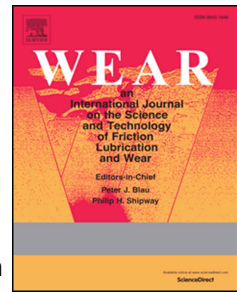
To appear in: Wear

Received Date: 3 March 2023 Revised Date: 19 June 2023 Accepted Date: 21 June 2023

Please cite this article as: Z. Zhang, Y. Ling, J. Hui, F. Yang, X. Zhang, S. Tan, Z. Xie, F. Fang, Effect of C additions to the microstructure and wear behaviour of CoCrFeNi high-entropy alloy, *Wear* (2023), doi: https://doi.org/10.1016/j.wear.2023.205032.

This is a PDF file of an article that has undergone enhancements after acceptance, such as the addition of a cover page and metadata, and formatting for readability, but it is not yet the definitive version of record. This version will undergo additional copyediting, typesetting and review before it is published in its final form, but we are providing this version to give early visibility of the article. Please note that, during the production process, errors may be discovered which could affect the content, and all legal disclaimers that apply to the journal pertain.

© 2023 Published by Elsevier B.V.



Effect of C additions to the microstructure and wear behaviour of

CoCrFeNi high-entropy alloy

Zeling Zhang<sup>a</sup>, Yanfang Ling<sup>a</sup>, Jia Hui<sup>a</sup>, Fei Yang<sup>a</sup>, Xuhai Zhang<sup>a</sup>, Shuyong Tan<sup>b</sup>,

Zonghan Xiec,d, Feng Fanga,\*

<sup>a</sup> Jiangsu Key Laboratory of Advanced Metallic Materials, Southeast University, Nanjing 211189, China

<sup>b</sup> School of Materials Science and Engineering, Nanjing Institute of Technology, Nanjing 211167, China

<sup>c</sup> School of Mechanical Engineering, University of Adelaide, Adelaide SA 5005, Australia

<sup>d</sup> School of Engineering, Edith Cowan University, Joondalup WA 6027, Australia

\*Corresponding authors:

**Feng FANG:** 

Tel.: 86-25-52090630; Email address: fangfeng@seu.edu.cn;

Address: School of Materials Science and Engineering, Southeast University,

Jiangning District, Nanjing, 211189, China

**ABSTRACT** 

CoCrFeNi high entropy alloys (HEAs) suffer from inferior hardness and low wear resistance.

The introduction of hard particles is a common strategy to improve the tribological properties

of this kind of alloy. However, the influence of carbide type (M23C6, M7C3, and M3C2) and its

volume fraction on wear resistance is still under debate. In this work, (CoCrFeNi)<sub>100-x</sub>Cx (x=

0, 1.3, 1.7, 3.5, and 5.4 at. %) HEAs were prepared by vacuum arc melting. M<sub>23</sub>C<sub>6</sub> precipitated

in the FCC matrix through a subsequent heat treatment process. The effect of carbon additions

on the microstructural evolution and wear behavior of (CoCrFeNi)100-xCx HEAs was

investigated by dry sliding experiments with Al<sub>2</sub>O<sub>3</sub> ceramic balls as counterparts. The results

show that the C interstitials increased the lattice constant of the FCC matrix, on the other hand, the size and volume fraction of carbide precipitates increased with the carbon content. The Cr<sub>23</sub>C<sub>6</sub> precipitates appeared at the grain boundaries and interdendritic regions, which is believed to help strengthen the alloy, leading to an increase in its hardness and wear resistance. However, when the C content is greater than 0.28 wt %, the wear rate went up due to the poor toughness and severe three-body abrasive wear.

**Keywords:** High entropy alloys (HEA); CoCrFeNi; M<sub>23</sub>C<sub>6</sub> precipitation; Microstructure; Wear resistance

# 1. Introduction

CoCrFeMnNi equiatomic multicomponent single-phase alloys, also known as Cantor alloys, were first proposed in 2004 [1] [2]. A recent study showed that CoCrFeNi may have better wear resistance than Cantor alloys due to its higher hardness [3]. Moreover, in vacuum CoCrFeNi has attracted much interest, since its wear resistance is superior or comparable to steel and some intermetallics [4]. Unfortunately, CoCrFeNi, one of classical high entropy alloys (HEAs), has been reported to have high wear rates ranging from 2.3×10<sup>-4</sup> to 13.6×10<sup>-4</sup> mm<sup>3</sup>·N<sup>-1</sup>·m<sup>-1</sup> at room temperature [5], which limits its engineering applications. Taking a cue from steel design, in which carbon is commonly used to enhance wear resistance by solid solution and precipitation strengthening [8], elemental doping or hard particle inclusions is considered to be a viable technique to enhance the wear resistance of HEAs [6,7]. For example, Guo et al. [9] added Cr<sub>3</sub>C<sub>2</sub> to CoCrFeNiMn HEA to produce wear-resistant composites using the SPS

technique. The resulting composites are composed of two distinct phases: the FCC phase as the matrix and the Cr<sub>7</sub>C<sub>3</sub> phase as reinforcement. The formation of the M<sub>7</sub>C<sub>3</sub> hard particulates is believed to be one of the main reasons for the improved wear resistance [10–12]. There are fewer studies on the wear resistance of FCC HEAs containing M<sub>23</sub>C<sub>6</sub> phase. Heat treatment can be used to alter the carbide type in the alloys, for instance from Cr<sub>7</sub>C<sub>3</sub> to Cr<sub>23</sub>C<sub>6</sub> [13]. It is worth noting that the carbide structure in C-doped high-entropy alloys may change during wear. However, the influence of carbide type (M<sub>23</sub>C<sub>6</sub>, M<sub>7</sub>C<sub>3</sub>, and M<sub>3</sub>C<sub>2</sub>) and its volume fraction on the wear resistance of HEAs remains unsettled.

Increasing the carbon content can promote the precipitation of the carbide phase. Chen et al. [14] reported that with increasing carbon content, (Fe<sub>50</sub>Mn<sub>30</sub>Co<sub>10</sub>Cr<sub>10</sub>)<sub>100-x</sub>C<sub>x</sub> HEAs changes from single-phase FCC to the FCC+ M<sub>23</sub>C<sub>6</sub> phase. As a result, the microhardness and yield strength of FCC+ M<sub>23</sub>C<sub>6</sub> phases HEAs were significantly improved. In this work, a series of (CoCrFeNi)<sub>100-x</sub>C<sub>x</sub> (x=0, 1.3, 1.7, 3.5, and 5.4 at.%) HEAs were prepared by arc melting technique. Then heat treatment was applied to induce the formation of M<sub>23</sub>C<sub>6</sub> particulates in the CoCrFeNi matrix. The effects of C content on the microstructural development and wear resistance of (CoCrFeNi)<sub>100-x</sub>C<sub>x</sub> were investigated. The wear mechanism of CoCrFeNi-based composites was also ascertained.

# 2. Experimental

The raw materials used are Co, Cr, Fe, Ni, and C powders (purity≥99.99 wt.% for each type). CoCrFeNi HEAs with different carbon contents were prepared in a vacuum arc-melting furnace equipped with a water-cooled copper crucible (VAF-300, Nanjing Laibu Technology

Industrial Co., Ltd., Nanjing, P.R. China). During the fabrication process, HEA ingots were remelted five times to ensure composition homogeneity [15]. The as-cast HEAs ingot was placed in a chamber furnace and then annealed at 1100 °C for 6 h under argon atmosphere before quenching. The chemical compositions of the (CoCrFeNi)<sub>100-x</sub>C<sub>x</sub> alloys were determined by a direct reading spectrometer (MAXx LMF15, Spike Analytical Instruments, Germany) as shown in Table 1. The content of carbon in different samples was verified by the high-frequency carbon-sulphur analyzer (CS-2800, NCS Testing Technology Co., Ltd., Beijing, P.R.China), which is 0 at.%, 1.3 at.%, 1.7 at.%, 3.5 at.%, and 5.4 at.%. For convenience and clarity, the (CoCrFeNi)<sub>100-x</sub>Cx alloys with x =0 at. %, 1.3 at.%, 1.7 at.%, 3.5 at.%, and 5.4 at.% are designated as C00, C13, C17, C35 and C54, respectively.

**Table 1** Chemical composition (wt.%) of (CoCrFeNi)<sub>100-x</sub>C<sub>x</sub> alloys.

|    | C00   | C13   | C17   | C35   | C54   |
|----|-------|-------|-------|-------|-------|
| Co | 26.14 | 26.06 | 26.04 | 25.94 | 25.82 |
| Cr | 23.06 | 23.00 | 22.98 | 22.88 | 22.78 |
| Fe | 24.77 | 24.70 | 24.68 | 24.58 | 24.47 |
| Ni | 26.03 | 25.96 | 25.94 | 25.83 | 25.72 |
| C  | 1     | 0.28  | 0.37  | 0.77  | 1.20  |

The microstructure was observed by an optical microscope (OM, MV5000, Nanjing Lianchuang Analytical Instrument Co., LTD, Nanjing, P.R.China) and also a field-emission scanning electron microscope (SEM, FEI Sirion 200, FEI Company, Hillsboro, Oregon, USA). The Image-Pro Plus software was used to determine the volume fraction of the carbide phase in the HEAs. The chemical compositions were identified by energy dispersive spectrometry (EDS, NordlysMax3, Oxford Instruments, Oxford, UK). The transmission electron microscope analysis (TEM, Talos F200X, Thermo Fisher Scientific, Waltham, Massachusetts, USA) was performed at an acceleration voltage of 200 kV. The crystal structure was characterized by an

X-ray diffractometer (XRD, SmartLab 3, Rigaku Corporation, Japan) with Cu K $\alpha$  radiation ( $\lambda$  = 0.154 nm) at a step size of 0.2°/min.

Microhardness tests were carried out using an automatic microhardness tester (FM-700, FUTURE-TECH CORP., Japan). The maximum load was 100 gf and the holding time was 15 s. Ten measurement points were selected from the edge to the core to calculate the average hardness. The wear behaviour of the (CoCrFeNi)<sub>100-x</sub>C<sub>x</sub> alloys under the dry sliding condition was examined using a ball on disk wear-testing machine (HT-1000, Lanzhou Zhongke Kaihua Technology Development Co., Ltd., Lanzhou, P.R.China). The wear test setup is schematically illustrated in Fig. 1. Al<sub>2</sub>O<sub>3</sub> ceramic balls (Al<sub>2</sub>O<sub>3</sub>:93%, SiO<sub>2</sub>:5%, HD-6, AS ONE CORPORATION, Japan) with a diameter (D) of 6 mm were chosen as counter body material because of their high microhardness (HV1000) and weak interfacial bonding at the real contact area. The average friction coefficient could be affected by surface roughness [16]. The sample used for the friction test is a 12 mm×12 mm×1 mm flake, which was polished with 240#, 400#, 800#, 1200#, 1500#, 2000# sandpaper and the diamond paste with the particle size of 0.5 μm. The surface profilometer (Dektak 150, Bruker Daltonic Inc, Germany) was used to measure the surface roughness of the samples and the cross-sectional profile of the worn track. As shown in Fig. 2, the average roughness of the sample surface before the wear test (Ra) was found to be less than 10 nm. The wear test time was 30 min, and the diameter (d) of the wear track was 6 mm. According to the literature [17], the wear rate (K) of the HEAs can be calculated by the Archard law, i.e., Eq. (1):

$$K = \frac{V}{L \times F} = \frac{A \times d \times \pi}{n \times d \times \pi \times F} = \frac{A}{n \times F}$$
 (1)

where "V" is the total wear volume, "L" is the travel distance of the sliding ball, "F" is the normal load, "A" is the cross-sectional area of the worn track, "d" is the diameter of the wear trace, "n" is the number of sliding cycles run by the alumina ball. Therefore, the wear rate is proportional to the two-dimensional cross-sectional area of the wear track (A) determined using a surface profilometer [18–21]. Due to  $V=A\times d\times \pi$ , the volume loss (V) can be easily obtained. The accuracy of the results can be improved by multiple measurements of A at various locations. For that, each worn sample was measured 3 times by rotating 120° at each time. The average value of the cross-sectional area was used to calculate the wear rate. AISI 304 with a hardness of 245 HV is commonly used as a benchmark for the wear resistance of FCC structured high entropy alloys [22]. Therefore, we measured the tribological properties of AISI 304 and then compared them with the materials prepared in this paper.

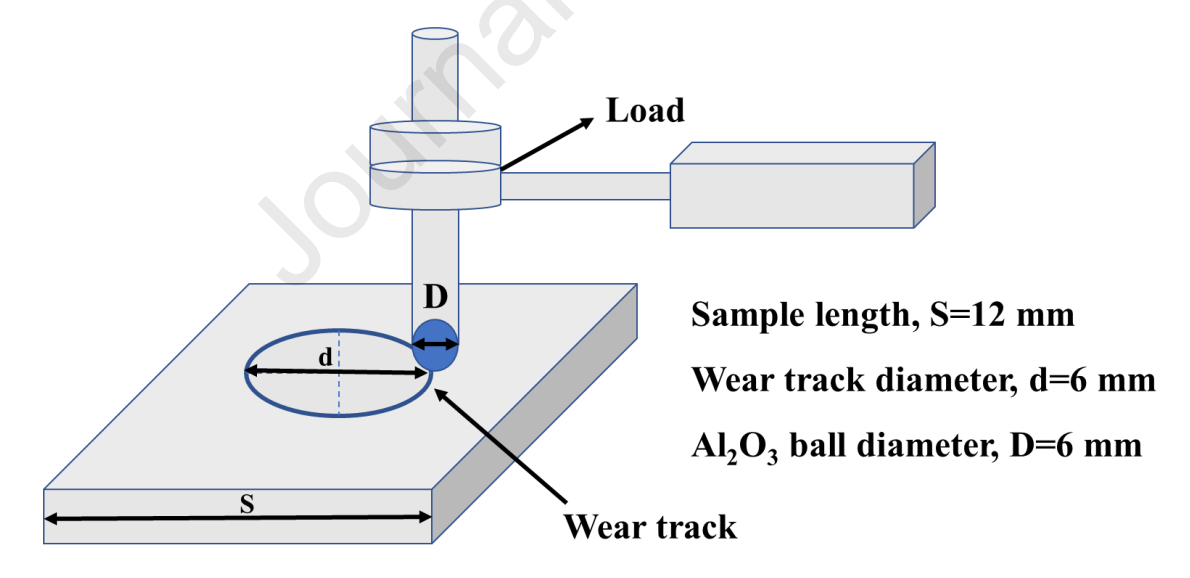


Fig. 1. Schematic diagram of the ball-on-disc sliding wear test set-up.

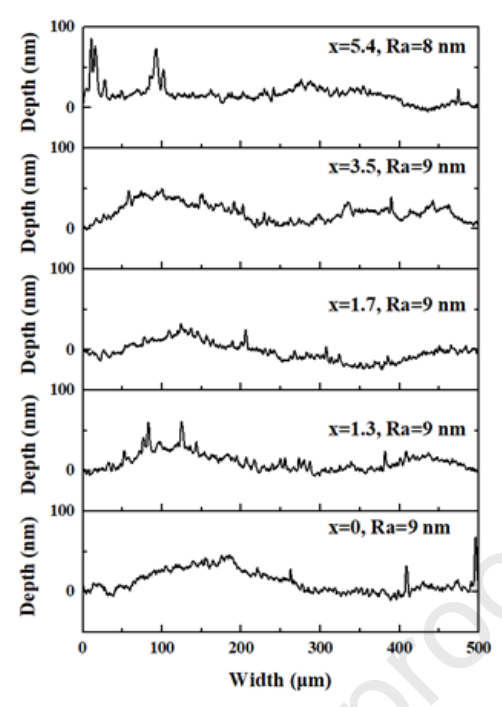


Fig. 2 The average surface roughness ( $R_a$ ) of (CoCrFeNi)<sub>100-x</sub>C<sub>x</sub> (x=0,1.3,1.7,3.5,5.4) before the wear tests.

### 3. Results and discussion

### 3.1. Microstructure and chemical composition of (CoCrFeNi)<sub>100-X</sub>C<sub>X</sub> alloys

The carbon content showed a marked influence on the microstructural evolution of the CoCrFeNi HEAs. As observed from Fig. 3(a), the CoCrFeNi HEA is a single-phase alloy with grain boundaries that are clearly visible. With the increase in carbon content, the dendrite (DR) and inter-dendrite (ID) structures became predominant (Fig. 3(b-d) insert). The DR regions were made of the matrix and the ID regions were of the carbides (Fig. 3(b-d)). The high-angle grain boundaries with high interfacial energy could act as the preferred sites for the precipitation of carbides [23]. As the carbon content exceeded the limit of solid solubility, the bright-white carbides precipitated along the grain boundaries forming long chains (Fig. 3(b-d)). The carbides precipitated at grain boundaries can hinder the movement of grain boundaries, thus limiting the growth of grains. In addition, the driving force of atomic diffusion in HEAs is insufficient, so the carbides will also precipitate in the DR region [24–28]. Generally speaking, the volume fraction of carbide increased with an increase in C content: the volume fraction of carbide phase is found to be 2%, 3%, 16%, and 22% in the C13, C17, C35, and C54 alloys, respectively.

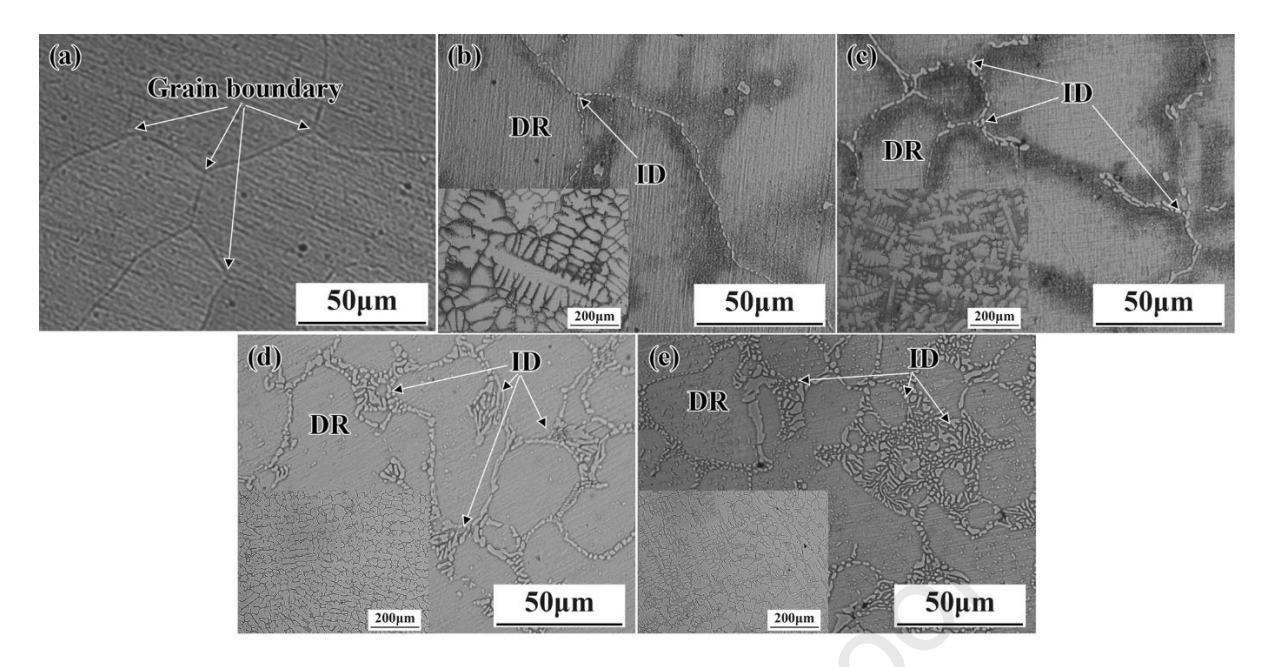


Fig. 3. Optical micrographs of the (CoCrFeNi)<sub>100-x</sub>C<sub>x</sub> alloys: (a) C00; (b) C13; (c) C17; (d) C35 and (e) C54.

The elemental maps (Fig. 4) and detailed chemical composition (Table 2) from the EDS analysis revealed that the segregation of Cr and C elements took place, leading to the formation of carbide particles. The phenomenon can be explained by the mixing enthalpy value of different atom pairs. The negative mixing enthalpy between Cr and C atoms (-61 kJ/mol) resulted in a stronger atomic affinity than the other metal elements with carbon [14].

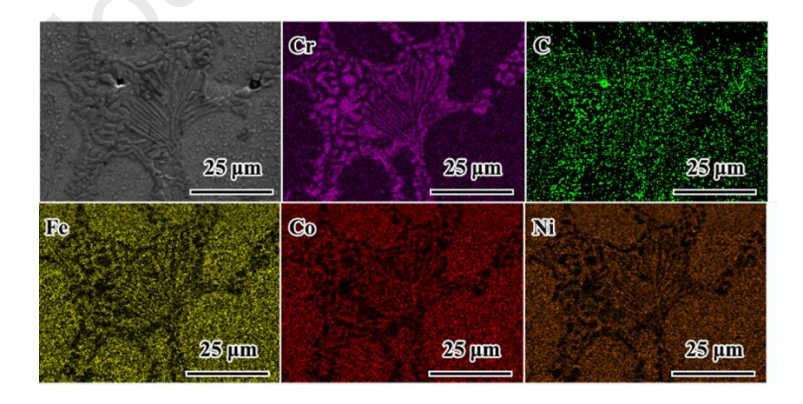


Fig. 4. SEM image and corresponding elemental distribution maps of the (CoCrFeNi)<sub>94.6</sub>C<sub>5.4</sub> alloy.

**Table 2** Chemical composition (at. %) of the (CoCrFeNi)<sub>100-x</sub>C<sub>x</sub> alloys prepared in this work.

| Alloy ID | Region | Co   | Cr   | Fe   | Ni   | С |
|----------|--------|------|------|------|------|---|
| C00      | Matrix | 25.4 | 25.5 | 24.7 | 24.4 | / |

| C13 | Matrix  | 21.7 | 20.2 | 21.5 | 21.0 | 15.6 |
|-----|---------|------|------|------|------|------|
| CIS | Carbide | 7.5  | 48.4 | 9.4  | 6.0  | 28.7 |
| C17 | Matrix  | 22.9 | 17.7 | 22.1 | 22.0 | 15.3 |
| CI/ | Carbide | 8.4  | 44.7 | 9.5  | 6.6  | 30.8 |
| C35 | Matrix  | 23.3 | 15.2 | 22.5 | 22.9 | 17.0 |
| C33 | Carbide | 4.6  | 48.9 | 7.0  | 1.7  | 37.8 |
| C54 | Matrix  | 21.3 | 19.1 | 20.9 | 20.1 | 18.6 |
|     | Carbide | 4.4  | 49.1 | 6.0  | 2.9  | 37.6 |

To ascertain the crystal structure of carbides, the TEM images of C17 were obtained. Both needle-like and granular precipitates appear to be densely packed in the alloys (Fig. 5(a, c)). The selected area electron diffraction (SAED) patterns (Fig. 5(b, d)) indicate that the Cr- and C-rich precipitates are indeed M<sub>23</sub>C<sub>6</sub> carbide. Fig. 5(d) also shows that the M<sub>23</sub>C<sub>6</sub> carbide and the matrix have a lattice parameter ratio of about 3:1, and the carbide phase has developed an orientation relationship with the matrix of (111)M<sub>23</sub>C<sub>6</sub>// (111)matrix and [011]M<sub>23</sub>C<sub>6</sub>// [011]matrix.

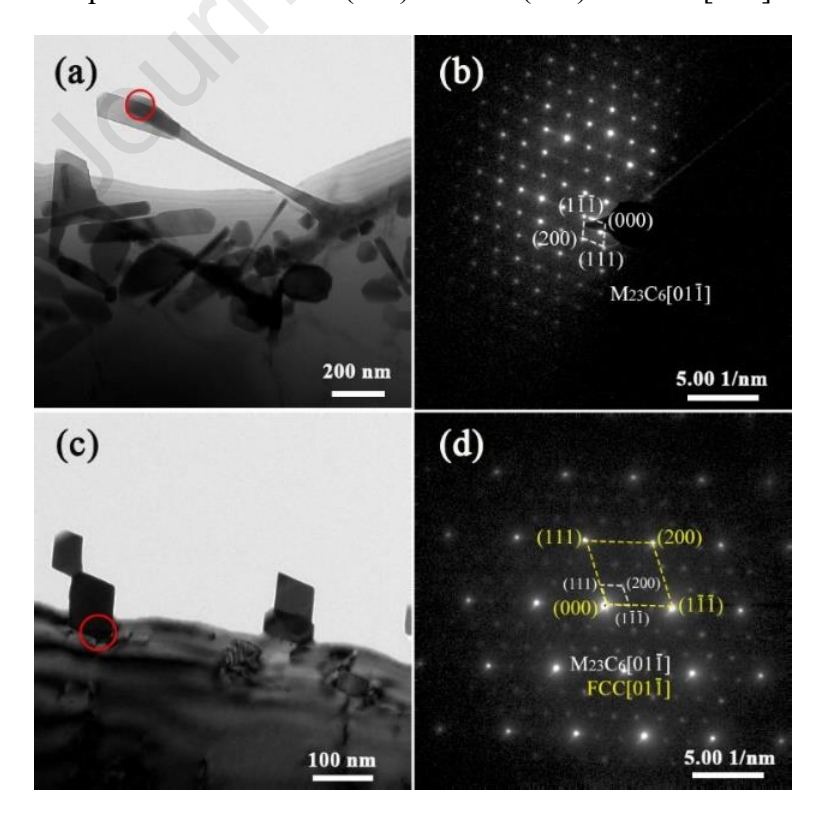


**Fig. 5.** TEM images and structural analysis of C17: (a) bright-field image and (b) the corresponding SAED pattern of needle-like precipitate, (c) bright-field image and (d) the corresponding SAED pattern of the granular precipitate and matrix.

### 3.2. XRD characterization

The XRD patterns of the (CoCrFeNi)<sub>100-x</sub>C<sub>x</sub> alloys with different carbon contents are shown in Fig. 6(a). The results suggest that the FCC phase was the main one in the HEAs. The diffraction peaks at 42.7°, 51.0°, and 75.2° are corresponding to the (100), (200), and (220) crystal planes of the FCC matrix phase, respectively. However, due to the low content, the carbide phases cannot be detected by XRD. Fig. 6(b) is the close-up view of the (200) diffraction peak of the FCC phase. Notably, the (200) diffraction peak shifted towards a lower 20 angle with an increase in the carbon content from 0 to 1.3 %. However, a further increase in the carbon content caused the (200) diffraction peak to shift back toward a higher 20 angle. Similar phenomena have been reported in (CoCrFeNi)C<sub>x</sub> alloy [26], and (CoCrFeMnNi)<sub>100-x</sub>C<sub>x</sub> alloy [24]. For (CoCrFeNi)<sub>100-x</sub>C<sub>x</sub> alloys, the lattice constants of the FCC phase were estimated from (200) diffraction peaks to be 3.570 Å, 3.574 Å, 3.573 Å, 3.572 Å, and 3.572 Å, respectively. In general, the addition of carbon increased the lattice constant of CoCrFeNi HEAs due to the dissolution of C into the FCC phase.

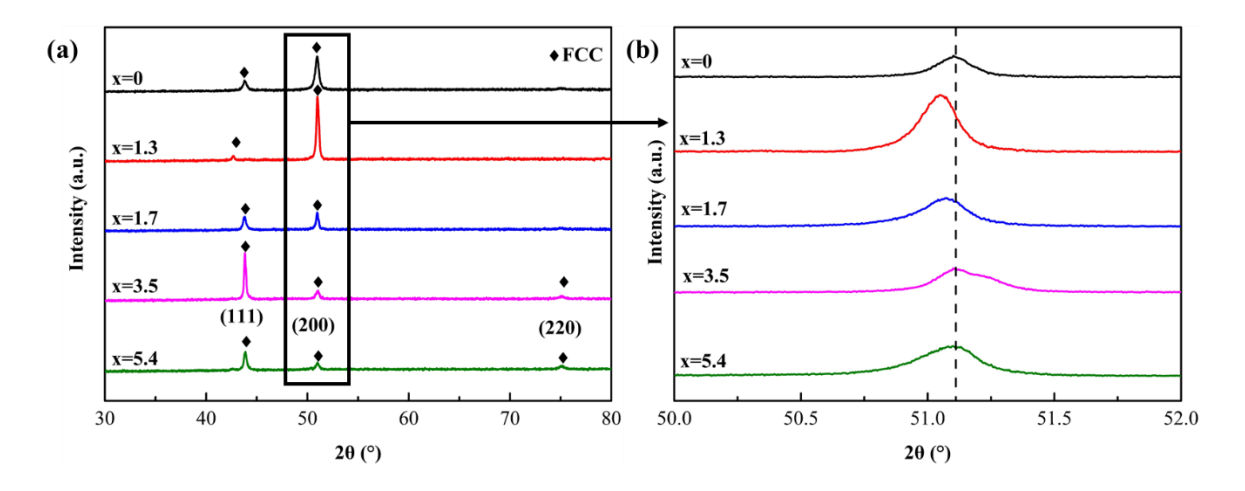


**Fig.6.** (a) XRD patterns of  $(CoCrFeNi)_{100-x}C_x$  alloys; (b) an enlarged view for the (200) diffraction peak of FCC phase in the  $(CoCrFeNi)_{100-x}C_x$  alloys.

### 3.3. Hardness

The average Vickers hardness value of  $(CoCrFeNi)_{100-x}C_x$  alloys was found to gradually increase from 174 HV to 273 HV with the increase of C content (Fig. 7). The enhancement in hardness is mainly due to grain refinement and the pinning effect of carbide particles [29] as well as the formation of a dendritic (DR) network [23].

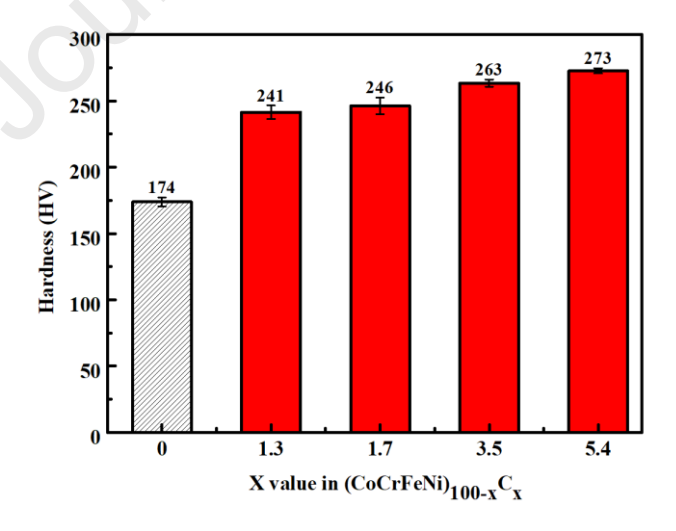
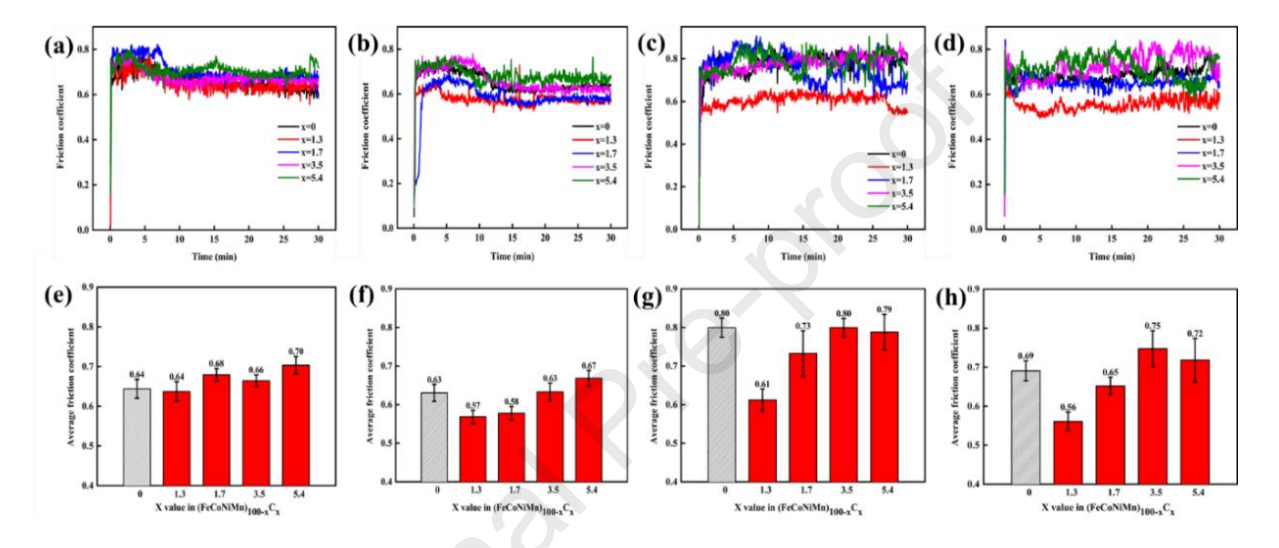


Fig. 7. Vickers hardness values of  $(CoCrFeNi)_{100-x}C_x$  alloys. The error bars represent the standard deviation.

### 3.4. Friction coefficient and volumetric wear rate

Fig. 8(a-d) shows the friction coefficient for (CoCrFeNi)<sub>100-x</sub>C<sub>x</sub> alloys as a function of

sliding time. The friction coefficient reached a steady state at ~10 min, so the friction coefficient between 10 and 30 min was used to calculate the average friction coefficient. Fig. 8(e-h) demonstrates the average friction coefficients of the new alloys with different carbon content. It can be seen that the average friction coefficient decreased after initial carbon doping. However, with the further increase in carbon content, the average friction coefficient showed an overall upward trend.



**Fig. 8.** Friction coefficient for (CoCrFeNi)<sub>100-X</sub>C<sub>X</sub> alloys as a function of the wear test time: (a) v=100 mm/s, F=6.5 N, (b) v=100 mm/s, F=11.5 N, (c) v=200 mm/s, F=6.5 N, (d) v=300 mm/s, F=6.5 N; Average friction coefficient of (CoCrFeNi)<sub>100-X</sub>C<sub>X</sub> alloys: (e) v=100 mm/s, F=6.5 N, (f) v=100 mm/s, F=11.5 N, (g) v=200 mm/s, F=6.5 N, (h) v=300 mm/s, F=6.5 N. The error bars represented the standard deviation.

Fig. 9(a-d) present the typical cross-sectional profiles of wear tracks in (CoCrFeNi)<sub>100-x</sub>Cx alloys. The CoCrFeNi alloy exhibits the largest cross-sectional area of the worn track, while the C13 shows the lowest wear loss. In addition, both the depth and width of the wear track increased with the increase in normal load and sliding velocity. Fig. 9(e-h) depicts the volumetric wear rate of (CoCrFeNi)<sub>100-x</sub>Cx HEAs under different test conditions. The wear rate of (CoCrFeNi)<sub>100-x</sub>Cx HEAs decreased after initial carbon doping. However, as the carbon

content increases, the wear rate kept rising. The results show that the proper introduction of carbide particles is key to improving the wear resistance of the CoCrFeNi alloy.

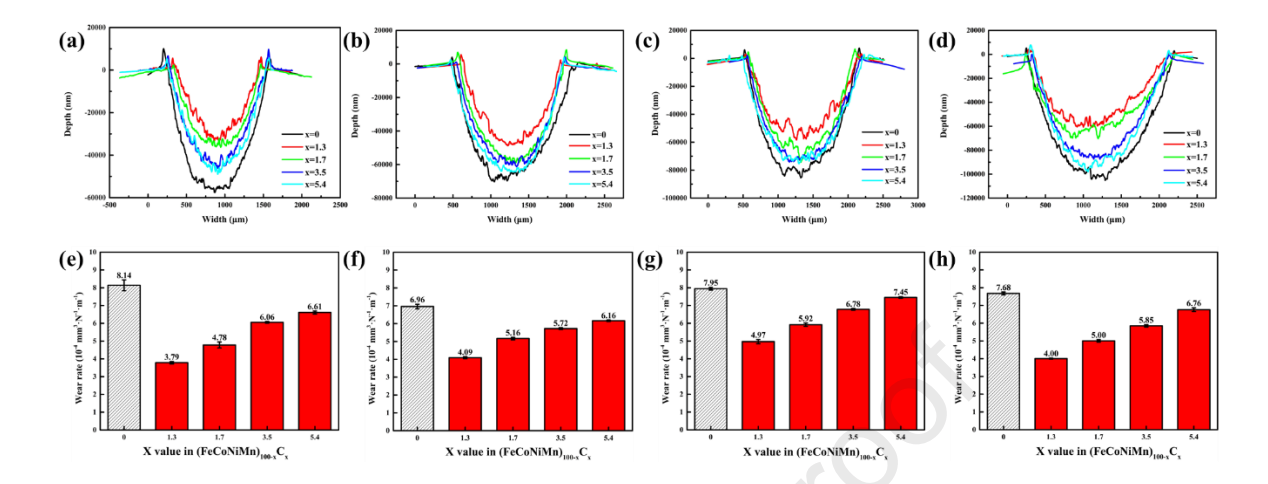


**Fig. 9.** The cross-sectional wear track profiles of  $(CoCrFeNi)_{100-x}C_X$  alloys: (a) v=100 mm/s, F=6.5 N, (b) v=100 mm/s, F=11.5 N, (c) v=200 mm/s, F=6.5 N, (d) v=300 mm/s, F=6.5 N; Volumetric wear rate of  $(CoCrFeNi)_{100-x}C_X$  alloys: (e) v=100 mm/s, F=6.5 N, (f) v=100 mm/s, F=11.5 N, (g) v=200 mm/s, F=6.5 N, (h) v=300 mm/s, F=6.5 N. The error bars represented the standard error of the arithmetic mean.

Besides, we measured the tribological properties of AISI 304 (v=100 mm/s, F=6.5 N) and compared them with the materials prepared in this paper. The results show that the friction coefficient and wear rate of AISI 304 are 0.45 and 1.64×10<sup>-4</sup> mm<sup>3</sup>·N<sup>-1</sup>·m<sup>-1</sup>, respectively. This indicates that although carbon additions can improve the wear resistance of CoCrFeNi in air at room temperature, the wear rate of (CoCrFeNi)<sub>100-x</sub>C<sub>x</sub> is still higher than that of AISI 304 in the same condition. However, the wear resistance of CoCrFeNi in a vacuum is superior or comparable to steel [4]. Therefore, this investigation necessitates the future study of the tribological behaviour of C-doped high-entropy alloys in vacuum, presumably for aerospace applications [4]. Under the condition of a normal load of 6.5 N and sliding velocity of 100 mm/s, the volumetric wear loss is lowest, which is consistent with the experimental observations. Therefore, in this case, the influence of carbon content on the wear resistance of CoCrFeNi high entropy alloy is analyzed.

### 3.5 Worn surface and debris characterization

Wear debris was examined after the wear tests, as shown in Fig. 10. The distribution of the wear debris size is over a broad range, with granular debris smaller than 5  $\mu$ m and flake-like debris larger than 10  $\mu$ m. The flake debris was generated due to the delamination of the layer from the worn surface, while the granular debris was formed by crushing the sheet-like debris or the abrasive wear [11]. As shown in Fig.10(a), the size of some flake debris can reach 30  $\mu$ m in C00. The large size of the flake debris often indicates a serious wear damage, where deep grooves may appear on the worn surface.

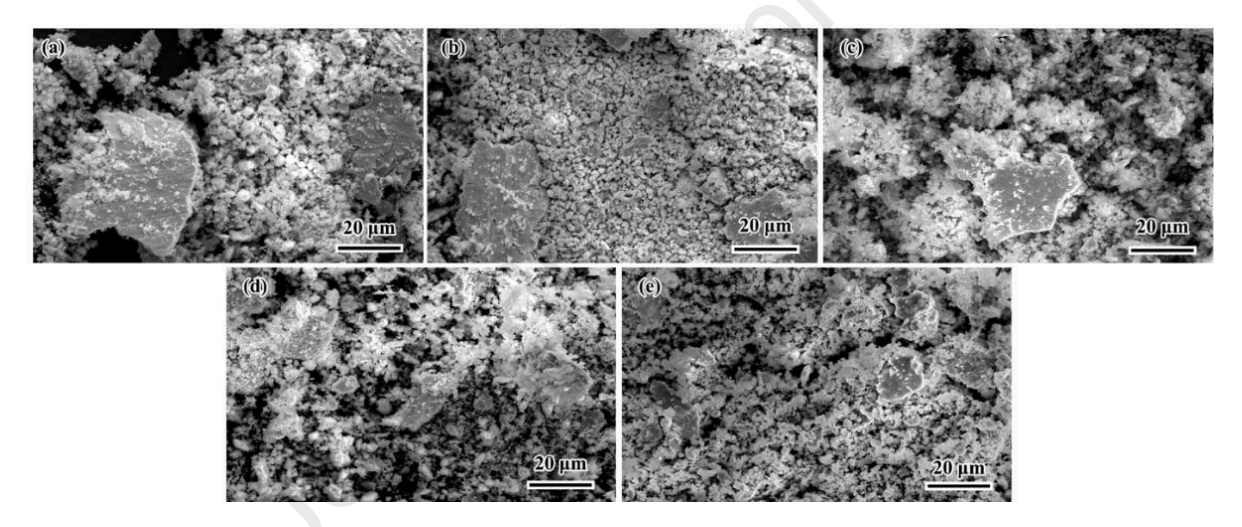


**Fig. 10.** SEM images of the wear debris of (CoCrFeNi)<sub>100-X</sub>C<sub>X</sub> alloys tested under a normal load of 6.5 N and a sliding velocity of 100 mm/s: (a) C00; (b) C13; (c) C17; (d) C35 and (e) C54.

Fig. 11 shows the surface morphology of the wear tracks of (CoCrFeNi)<sub>100-x</sub>C<sub>x</sub> alloys. Copious debris and numerous grooves were observed on the worn surfaces. The ploughing grooves along the sliding direction are the typical characteristic of abrasive wear. A comparison of Fig.11 (a, b) shows that the groove of C13 became shallower and, at the same time, the wear debris was reduced. This may explain the results that the friction coefficient has changed little and the wear rate decreased by adding 1.3 at.% carbon (Fig. 8 (e) and Fig. 9 (e)). With the

addition of carbon, the hardness of C13 increased (Fig. 7), so the wear rate decreased. Conventionally, the friction coefficient might also be reduced. However, the rough surface of C00 could gather a lot of wear debris that produced a lubricating effect, so the friction coefficient is equivalent to the C13 (Fig. 11(a)). Besides, the glaze layer appeared on the wear surface of (CoCrFeNi)98.3C1.7 (Fig. 11(c)). The chemical composition at different positions over the wear surface of (CoCrFeNi)98.3C1.7 was analyzed by EDS (Table 3). The oxygen content of the glaze layer is higher than elsewhere on the grooves. Fig. 12 shows the SEM image of the typical wear surface of (CoCrFeNi)94.6C5.4 alloy and corresponding elemental distribution maps. Oxygen element is enriched in scattered debris, suggesting that oxidation occurred on the worn surface during sliding, which might be caused by the temperature rising at the frictional contact [11]. In addition, the size of the carbide particles on the wear surface is smaller than those seen in Fig. 4. It indicates that the ceramic phase was broken into small fragments under the frictional loading. During the sliding contact, the soft matrix was worn off first, and the hard carbide particles became exposed. The extruding carbide particles were then broken up from the matrix or pushed into the matrix. This may help explain the rising friction coefficient and wear rate with increasing carbon content in Fig. 8(e) and Fig. 9(e). This phenomenon is commonly seen in some tribological studies involving the introducing of hard particles to enhance wear resistance [30].

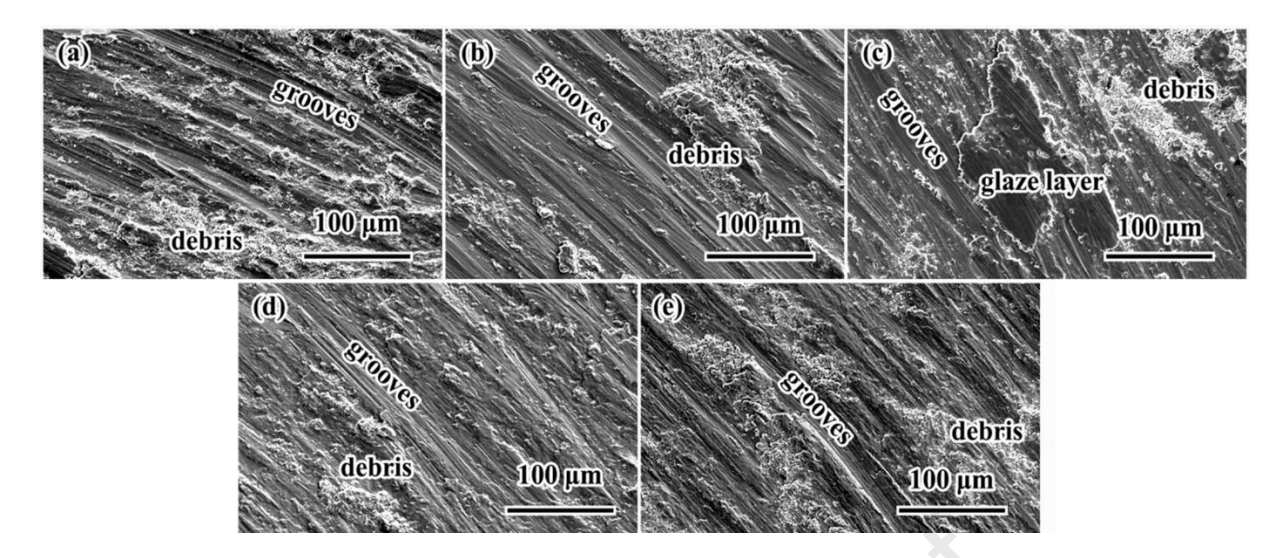


**Fig. 11.** SEM images of the wear surface of (CoCrFeNi)<sub>100-x</sub>C<sub>x</sub> alloys tested under a normal load of 6.5 N and a sliding velocity of 100 mm/s: (a) C00; (b) C13; (c) C17; (d) C35 and (e) C54.

**Table 3.** Chemical compositions (at. %) obtained at different positions on the wear surface of (CoCrFeNi)<sub>98.3</sub>C<sub>1.7</sub>.

| Position    | Со          | Cr   | Fe    | Ni       | С          | О    |
|-------------|-------------|------|-------|----------|------------|------|
| Grooves     | 22.6        | 20.8 | 21.9  | 22.0     | 9.2        | 3.5  |
| Glaze layer | 15.2        | 14.2 | 14.3  | 13.8     | 11.7       | 30.8 |
| 1           | ) (B)       | Юрт  | ලා    | 10 дип   | <b>N</b> 0 | ФД   |
| œ           |             | 0    |       | <u> </u> |            |      |
|             | <b>10</b> 0 | ım e | 10 рл | n        | ற்று       |      |

**Fig. 12.** SEM image of typical wear surface of (CoCrFeNi)<sub>94.6</sub>C<sub>5.4</sub> alloy and corresponding elemental distribution maps.

To further disclose the wear behavior of (CoCrFeNi)<sub>100-x</sub>C<sub>x</sub> alloys, the wear track cross-sectional profiles are presented in Fig. 13. Cracks initiation and propagation was observed to appear on the wear surface and the sub-surface for C35 and C54 samples (Fig. 13(d, e)). It is

believed that the increase in hardness resulting from solid solution strengthening and carbide formation has a negative impact on ductility [25,31]. Sacrificing ductility may accelerate crack initiation and propagation, thus resulting in a higher material loss (Fig. 9(e)). To better understand this wear mechanism and the oxidation process at room temperature, the cross-sectional examination of wear tracks after the wear testing was performed that included the EDS element mapping. The results show that the topmost layer is composed of compacted oxides (Fig. 14). In the present case, the outmost layer can work as a physical buffer to avoid the alloy and the Al<sub>2</sub>O<sub>3</sub> counterpart from contacting each other directly [4].

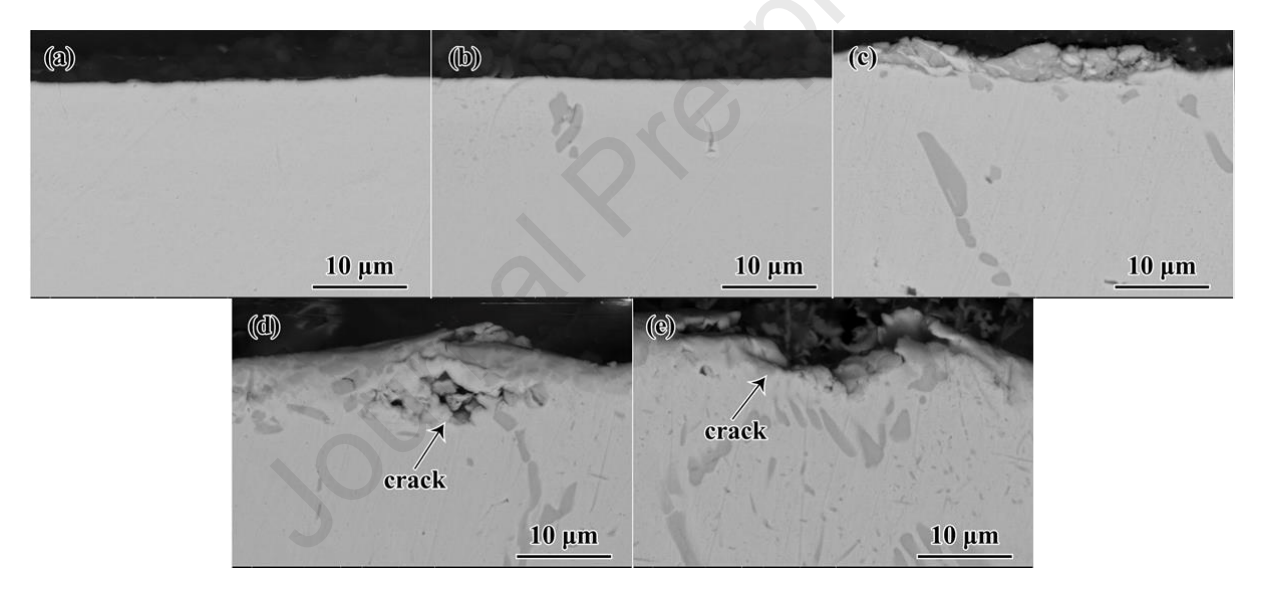


**Fig. 13.** SEM images of the cross-sections of the (CoCrFeNi)<sub>100-x</sub>C<sub>x</sub> alloys wear tracks tested under a normal load of 6.5 N and a sliding velocity of 100 mm/s: (a) C00; (b) C13; (c) C17; (d) C35 and (e) C54.

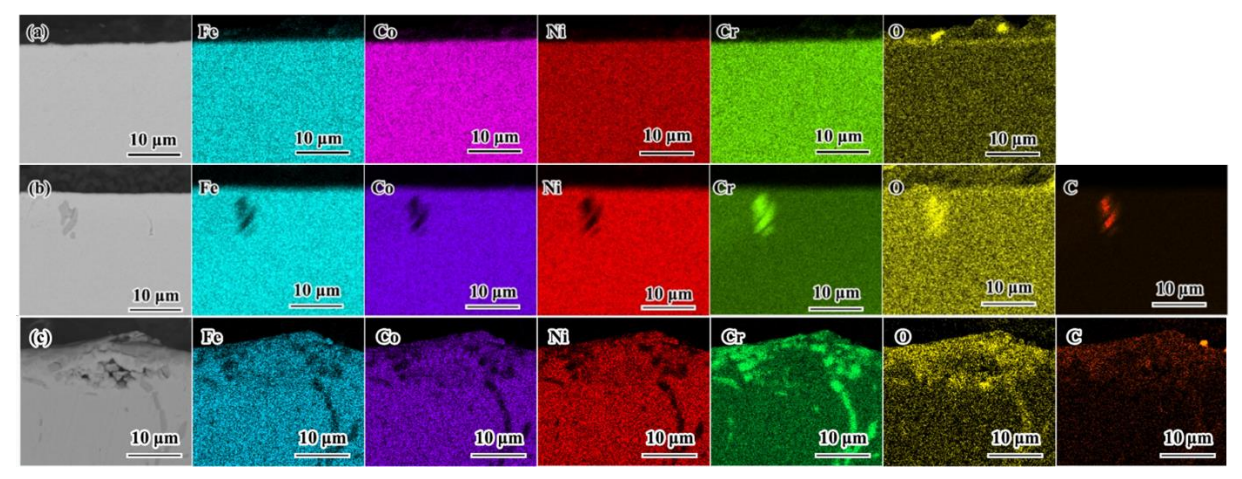


**Fig. 14.** SEM images of the wear track cross-sections of (CoCrFeNi)<sub>100-x</sub>C<sub>x</sub> alloys and the corresponding EDS mappings tested under a normal load of 6.5 N and a sliding velocity of 100 mm/s: (a) C00, (b) C13, (c) C35.

The wear scars of the Al<sub>2</sub>O<sub>3</sub> counterparts and corresponding element mapping are presented in Fig. 15 and Fig. 16, respectively. In Fig. 15(a), Al<sub>2</sub>O<sub>3</sub> counterparts were slightly worn, even though the hardness of the CoCrFeNi HEAs (273 HV) is far lower than that of the Al<sub>2</sub>O<sub>3</sub> counterparts (1000 HV). However, after adding carbon, cracks appeared on the surface of the Al<sub>2</sub>O<sub>3</sub> counterparts (Fig. 15(b-e)). This is due to the hardness of the carbide being about 1500 HV [32], slightly higher than the Al<sub>2</sub>O<sub>3</sub> ball. It suggests that the Al<sub>2</sub>O<sub>3</sub> ball not only abraded the matrix but also interacted with the second phase, which is consistent with the result of Fig. 12. The EDS results show that the transfer layer was generated on the worn surface of the Al<sub>2</sub>O<sub>3</sub> counterparts (Fig. 16(a)). Moreover, the transfer layer consists of a kind of oxide film (Fig. 16(b)). Xin et al. [16] reported that the transfer films were conducive to improving the wear resistance of the HEAs by re-distributing/lowering local stress and avoiding direct contact between the friction pairs.

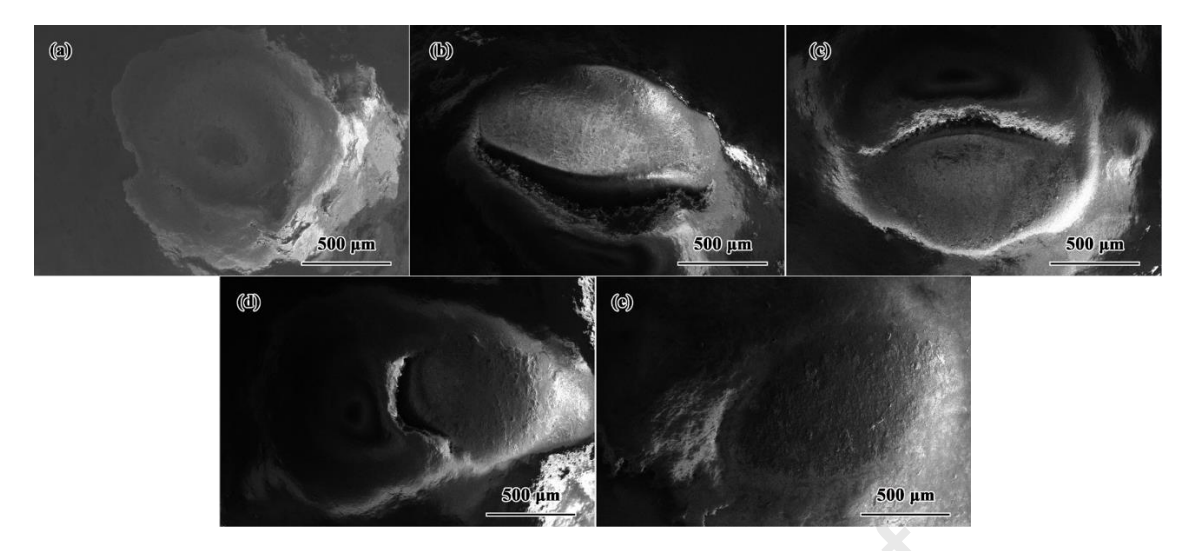


**Fig. 15.** Wear scars of Al<sub>2</sub>O<sub>3</sub> counterparts against the: (a) C00; (b) C13; (c) C17; (d) C35 and (e) C54 tested under a normal load of 6.5 N and a sliding velocity of 100 mm/s.

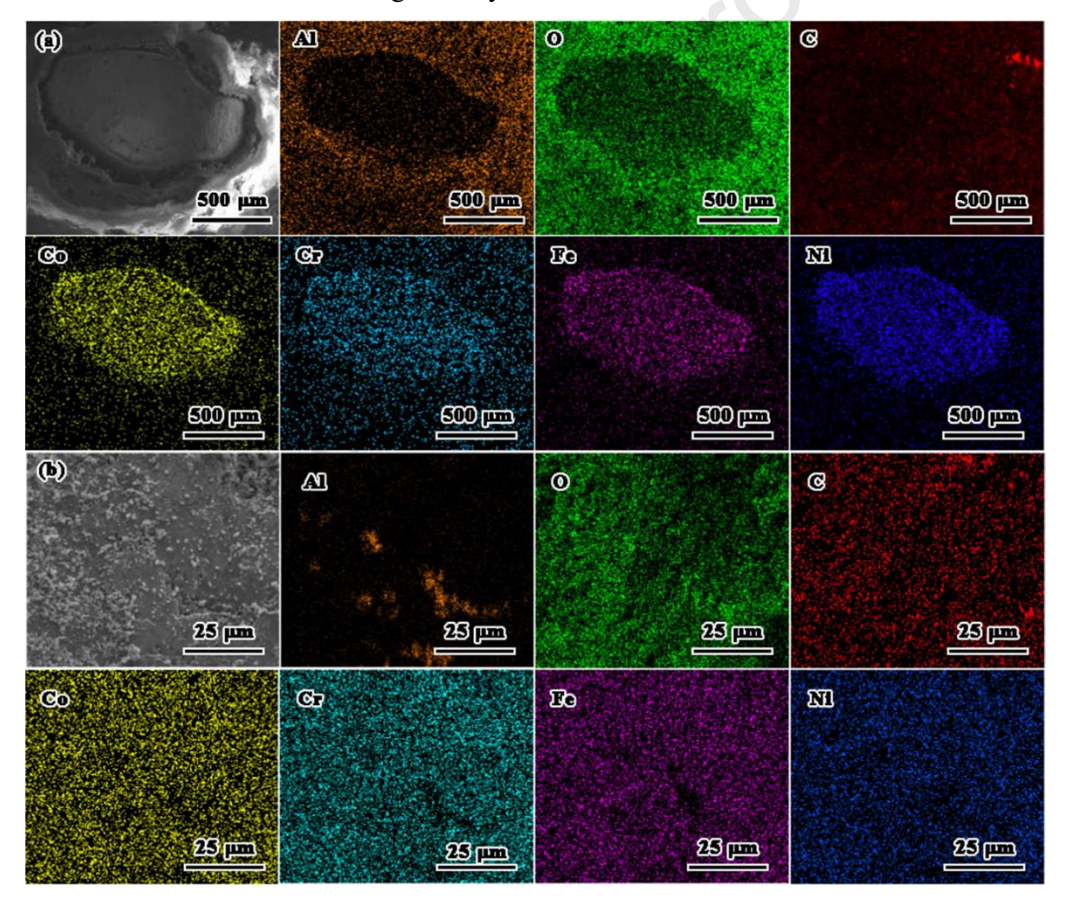


**Fig. 16.** The element mapping of wear scars of Al<sub>2</sub>O<sub>3</sub> counterparts against the C13 tested under a normal load of 6.5 N and a sliding velocity of 100 mm/s: (a) low magnification and (b) high magnification.

Similar worn surface morphologies suggest that no obvious wear mode transition occurred as the C content increased. It is evident that the major wear mechanism is abrasive wear (Fig.

11). Abrasion may also be induced by third-body particles such as fractured carbides as wear debris [33]. The wear mechanism of (CoCrFeNi)<sub>100-x</sub>C<sub>x</sub> alloy is shown in Fig. 17. A small number of carbide particles works to strengthen the alloy and reduces the degree of abrasive wear. However, with the increase in carbide content, carbide debris-assisted three-body abrasive wear could be aggravated. Cai et al. [29]reported that the abrasive wear caused by the shedding of hard carbides in the sliding contact could intensify the wear losses, which is consistent with the observation of this work. Furthermore, the negative effect of increased hardness on ductility may accelerate crack initiation and propagation, adding to the material loss. Therefore, the optimal C addition should be considered in maximizing the wear resistance of the CoCrFeNi alloy.

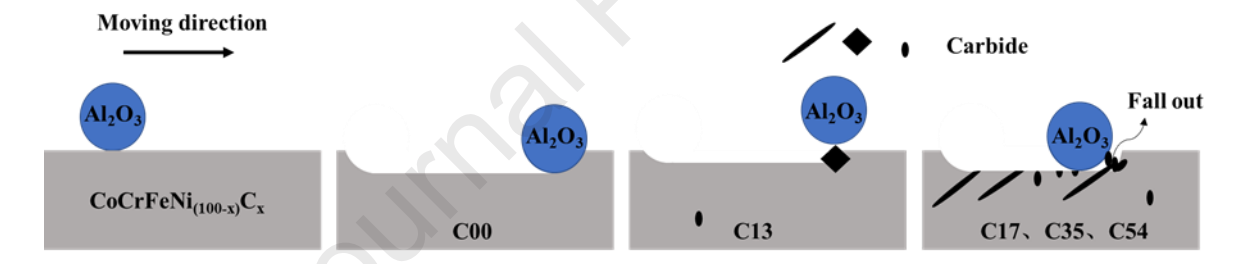


Fig. 17. The illustration of the wear process of (CoCrFeNi)<sub>100-x</sub>C<sub>x</sub> alloys at ambient conditions.

# 4. Conclusions

CoCrFeNi-based high entropy alloys with different carbon contents were prepared by arc melting. The effects of the C additions on the microstructure and wear resistance of the resultant alloys were investigated. The primary conclusions can be drawn as follows:

(1) The C interstitials in the FCC matrix increased the lattice constant. In addition, the Cr<sub>23</sub>C<sub>6</sub> precipitates appeared at the grain boundaries and interdendritic regions, which helped strengthen the allloy. The size and volume fraction of carbides increased with the carbon

content.

- (2) The C content has a significant effect on the room-temperature wear rate. When the C content is lower than 0.28 wt %, the wear rate dropped due to the improvement in alloy hardness. However, when the C content is higher than 0.28 wt %, the wear rate moved up due to the poor toughness and severe three-body abrasive wear.
- (3) With the increase of C content, the wear mode has no obvious change, with the main wear mechanism being abrasive wear. At room temperature, an oxide film was formed on the wear track, which is conducive to improving the wear resistance. Besides, the oxide film was detected on the Al<sub>2</sub>O<sub>3</sub> ball counterpart, indicative of the existence of the film transfer during the friction process.

# Acknowledgments

This work was supported by the National Natural Science Foundation of PR China (project no. 52171110) and the Jiangsu Key Laboratory of Advanced Metallic Materials, Southeast University, PR China (grant no. AMM2020A02), and also supported by the Science and Technology Advancement Program of Jiangsu Province, PR China (grant no. BA2022063).

### References

- [1] B. Cantor, I.T.H. Chang, P. Knight, A.J.B. Vincent, Microstructural development in equiatomic multicomponent alloys, Mater. Sci. Eng. A. 375–377 (2004) 213-218. https://doi.org/10.1016/j.msea.2003.10.257.
- [2] J.W. Yeh, S.K. Chen, S.J. Lin, J.Y. Gan, T.S. Chin, T.T. Shun, C.H. Tsau, S.Y. Chang, Nanostructured high-entropy alloys with multiple principal elements: Novel alloy design concepts and outcomes, Adv.

- Eng. Mater. 6 (2004) 299-303. https://doi.org/10.1002/adem.200300567.
- [3] Y. Tang, D.Y. Li, Nano-tribological behavior of high-entropy alloys CrMnFeCoNi and CrFeCoNi under different conditions: A molecular dynamics study, Wear. 476 (2021), 203583. https://doi.org/10.1016/j.wear.2020.203583.
- [4] Y. Geng, J. Chen, H. Tan, J. Cheng, J. Yang, W. Liu, Vacuum tribological behaviors of CoCrFeNi high entropy alloy at elevated temperatures, Wear. 456-457 (2020) 203368. https://doi.org/10.1016/j.wear.2020.203368.
- [5] A.K. Kasar, K. Scalaro, P.L. Menezes, Tribological properties of high-entropy alloys under dry conditions for a wide temperature range—a review, Materials. 14 (2021) 5814. https://doi.org/10.3390/ma14195814.
- [6] D. Liu, J. Zhao, Y. Li, W. Zhu, L. Lin, Effects of boron content on microstructure and wear properties of FeCoCrNiB<sub>x</sub> high-entropy alloy coating by laser cladding, Appl. Sci. 10 (2020) 49. https://doi.org/10.3390/app10010049.
- [7] Y. Yu, F. He, Z. Qiao, Z. Wang, W. Liu, J. Yang, Effects of temperature and microstructure on the triblogical properties of CoCrFeNiNb<sub>x</sub> eutectic high entropy alloys, J. Alloys Compd. 775 (2019) 1376-1385. https://doi.org/10.1016/j.jallcom.2018.10.138.
- [8] D. Bowden, Y. Krysiak, L. Palatinus, D. Tsivoulas, S. Plana-Ruiz, E. Sarakinou, U. Kolb, D. Stewart, M. Preuss, A high-strength silicide phase in a stainless steel alloy designed for wear-resistant applications, Nat. Commun. 9 (2018) 1374. https://doi.org/10.1038/s41467-018-03875-9.
- [9] Z. Guo, A. Zhang, J. Han, J. Meng, Microstructure, mechanical and tribological properties of CoCrFeNiMn high entropy alloy matrix composites with addition of Cr<sub>3</sub>C<sub>2</sub>, Tribol. Int. 151 (2020) 106436. https://doi.org/10.1016/j.triboint.2020.106436.
- [10] B. Han, Y. Chen, C. Tan, M. Jiang, J. Bi, J. Feng, X. Chen, L. Chen, L. Zhang, X. Liu, L. Cao, G. Bi, Microstructure and wear behavior of laser clad interstitial CoCrFeNi high entropy alloy coating reinforced by carbon nanotubes, Surf. Coat. Technol. 434 (2022) 128241. https://doi.org/10.1016/j.surfcoat.2022.128241.
- [11] J.K. Xiao, H. Tan, J. Chen, A. Martini, C. Zhang, Effect of carbon content on microstructure, hardness and wear resistance of CoCrFeMnNiC<sub>x</sub> high-entropy alloys, J. Alloys Compd. 847 (2020) 156533. https://doi.org/10.1016/j.jallcom.2020.156533.

- [12] T.D. Huang, L. Jiang, C.L. Zhang, H. Jiang, Y.P. Lu, T.J. Li, Effect of carbon addition on the microstructure and mechanical properties of CoCrFeNi high entropy alloy, Sci. China Technol. Sci. 61 (2018) 117-123. https://doi.org/10.1007/s11431-017-9134-6.
- [13] A.I. Gorunov, Investigation of M<sub>7</sub>C<sub>3</sub>, M<sub>23</sub>C<sub>6</sub> and M<sub>3</sub>C carbides synthesized on austenitic stainless steel and carbon fibers using laser metal deposition, Surf. Coat. Technol. 401 (2020) 126294. https://doi.org/10.1016/j.surfcoat.2020.126294.
- [14] L. Chen, Z. Li, P. Dai, P. Fu, J. Chen, Q. Tang, Effects of carbon addition on microstructure and mechanical properties of Fe<sub>50</sub>Mn<sub>30</sub>Co<sub>10</sub>Cr<sub>10</sub> high-entropy alloy prepared by powder metallurgy, J. Mater. Res. Technol. 20 (2022) 73–87. https://doi.org/https://doi.org/10.1016/j.jmrt.2022.07.067.
- [15] X.W. Liu, L. Liu, G. Liu, X.X. Wu, D.H. Lu, J.Q. Yao, W.M. Jiang, Z.T. Fan, W.B. Zhang, The role of carbon in grain refinement of cast CrFeCoNi high-entropy alloys, Metall. Mater. Trans. A. 49 (2018) 2151-2160. https://doi.org/10.1007/s11661-018-4549-8.
- [16] B. Xin, A. Zhang, J. Han, J. Meng, The tribological properties of carbon doped Al<sub>0.2</sub>Co<sub>1.5</sub>CrFeNi<sub>1.5</sub>Ti<sub>0.5</sub> high entropy alloys, Wear. 484–485 (2021) 204045. https://doi.org/10.1016/j.wear.2021.204045.
- [17] G. Deng, A.K. Tieu, X. Lan, L. Su, L. Wang, Q. Zhu, H. Zhu, Effects of normal load and velocity on the dry sliding tribological behaviour of CoCrFeNiMo<sub>0.2</sub> high entropy alloy, Tribol. Int. 144 (2020) 106116. https://doi.org/10.1016/j.triboint.2019.106116.
- [18] J. Lin, X. Zhang, Effects of racetrack magnetic field strength on structure and properties of amorphous carbon coatings deposited by HiPIMS using deep oscillation pulses, Surf. Coat. Technol. 438 (2022) 128417, https://doi.org/10.1016/j.surfcoat.2022.128417.
- [19] J. Lin, X. Zhang, P. Lee, R. Wei, Thick diamond like carbon coatings deposited by deep oscillation magnetron sputtering, Surf. Coat. Technol. 315 (2017) 294-302. https://doi.org/10.1016/j.surfcoat.2017.02.044.
- [20] J. Lin, R. Wei, F. Ge, Y. Li, X. Zhang, F. Huang, M. Lei, TiSiCN and TiAlVSiCN nanocomposite coatings deposited from Ti and Ti-6Al-4V targets, Surf. Coat. Technol. 336 (2018) 106-116. https://doi.org/10.1016/j.surfcoat.2017.10.009.
- [21] Z. Cheng, L. Yang, Z. Huang, T. Wan, M. Zhu, F. Ren, Achieving low wear in a μ-phase reinforced high-entropy alloy and associated subsurface microstructure evolution, Wear. 474–475 (2021) 203755. https://doi.org/10.1016/j.wear.2021.203755.

- [22] J. Joseph, N. Haghdadi, K. Shamlaye, P. Hodgson, M. Barnett, D. Fabijanic, The sliding wear behaviour of CoCrFeMnNi and AlxCoCrFeNi high entropy alloys at elevated temperatures, Wear. 428–429 (2019) 32-44. https://doi.org/10.1016/j.wear.2019.03.002.
- [23] Z. Xu, D.Y. Li, D.L. Chen, Effect of Ti on the wear behavior of AlCoCrFeNi high-entropy alloy during unidirectional and bi-directional sliding wear processes, Wear. 476 (2021) 203650. https://doi.org/10.1016/j.wear.2021.203650.
- [24] Y. Yu, B. Zhang, S. Zhu, Z. Zhang, W. Lu, T. Shen, Z. Wang, Microstructural and tribological characteristics of in situ induced chrome carbide strengthened CoCrFeMnNi high-entropy alloys, J. Mater. Eng. Perform. 29 (2020) 3714-3722. https://doi.org/10.1007/s11665-020-04872-0.
- [25] J. Chen, Z. Yao, X. Wang, Y. Lu, X. Wang, Y. Liu, X. Fan, Effect of C content on microstructure and tensile properties of as-cast CoCrFeMnNi high entropy alloy, Mater. Chem. Phys. 210 (2018) 136-145. https://doi.org/10.1016/j.matchemphys.2017.08.011.
- [26] L.J. Zhang, P.F. Yu, J.T. Fan, M.D. Zhang, C.Z. Zhang, H.Z. Cui, G. Li, Investigating the micro and nanomechanical properties of CoCrFeNi-C<sub>x</sub> high-entropy alloys containing eutectic carbides, Mater. Sci. Eng. A. 796 (2020) 140065. https://doi.org/10.1016/j.msea.2020.140065.
- [27] N.D. Stepanov, N.Y. Yurchenko, M.A. Tikhonovsky, G.A. Salishchev, Effect of carbon content and annealing on structure and hardness of the CoCrFeNiMn-based high entropy alloys, J. Alloys Compd. 687 (2016) 59-71. https://doi.org/10.1016/j.jallcom.2016.06.103.
- [28] J. Li, B. Gao, Y. Wang, X. Chen, Y. Xin, S. Tang, B. Liu, Y. Liu, M. Song, Microstructures and mechanical properties of nano carbides reinforced CoCrFeMnNi high entropy alloys, J. Alloys Compd. 792 (2019) 170-179. https://doi.org/10.1016/j.jallcom.2019.03.403.
- [29] Y. Cai, L. Zhu, Y. Cui, M. Shan, H. Li, Y. Xin, J. Han, Fracture and wear mechanisms of FeMnCrNiCo + x(TiC) composite high-entropy alloy cladding layers, Appl. Surf. Sci. 543 (2021) 148794. https://doi.org/10.1016/j.apsusc.2020.148794.
- [30] X. Deng, L. Huang, Q. Wang, T. Fu, Z. Wang, Three-body abrasion wear resistance of TiC-reinforced low-alloy abrasion-resistant martensitic steel under dry and wet sand conditions, Wear. 452–453 (2020) 203310. https://doi.org/10.1016/j.wear.2020.203310.
- [31] Z. Li, J. You, Y. Guo, C. Li, Y. Zhang, Z. Liu, Phase Transition Mechanism and Mechanical Properties of AlCrFe<sub>2</sub>Ni<sub>2</sub> High-Entropy Alloys with Changes in the Applied Carbon Content, Adv. Eng. Mater.

- 22 (2020) 1901363. https://doi.org/10.1002/adem.201901363.
- [32] K. Hirota, K. Mitani, M. Yoshinaka, O. Yamaguchi, Simultaneous synthesis and consolidation of chromium carbides (Cr<sub>3</sub>C<sub>2</sub>, Cr<sub>7</sub>C<sub>3</sub> and Cr<sub>23</sub>C<sub>6</sub>) by pulsed electric-current pressure sintering, Mater. Sci. Eng. A. 399 (2005) 154-160. https://doi.org/10.1016/j.msea.2005.02.062.
- [33] A. Chiba, K. Kumagai, N. Nomura, S. Miyakawa, Pin-on-disk wear behavior in a like-on-like configuration in a biological environment of high carbon cast and low carbon forged Co-29Cr-6Mo alloys, Acta Mater. 55 (2007) 1309-1318. https://doi.org/10.1016/j.actamat.2006.10.005.

## **Highlights**

- M<sub>23</sub>C<sub>6</sub> carbide reinforce CoCrFeNi high entropy alloys (HEAs) were prepared.
- The hardness of the HEAs increased with the carbon content.
- (CoCrFeNi)98.7C<sub>1.3</sub> HEA exhibited the lowest friction coefficient and wear rate.

| Dec | laration | of interests |  |
|-----|----------|--------------|--|
| DEC | iaralion | Of Interests |  |

| oxtimes The authors declare that they have no known competing financial interests or personal relationships that could have appeared to influence the work reported in this paper. |
|--|
| $\Box$ The authors declare the following financial interests/personal relationships which may be considered as potential competing interests:                                      |